Invoking the frequency dependence in square modulated light intensity techniques for the measurement of electron time constants in dye-sensitized solar cells

Hamid M. Ghaithan[a*], Saif M. Qaid[a], Mahmoud Hezam[b,c], Muhemmad B. Siddique[d], Idriss M. Bedja[e], Abdullah S. Aldwayyan[a]

[a] Physics and Astronomy Department, College of Science, King Saud University, P.O. Box 2455, Riyadh 11451, Saudi Arabia

[b] King Abdullah Institute for Nanotechnology, King Saud University, P.O. Box 2454, Riyadh 11451, Saudi Arabia

[c] Laboratory of Quantum Optoelectronics, Ecole Polytechnique Fédérale de Lausanne (EPFL), 1015 Lausanne, Switzerland

[d] Department of Physics, University of Management and Technology, Lahore, Pakistan

[e] Department of Optometry, College of Applied Medical Sciences, King Saud University, P.O. Box 10219, Riyadh 11433, Saudi Arabia

*Email address: hameedyemen1@gmail.com

Abstract

Dye-sensitized solar cells (DSSCs) have been considered as one of the most promising new generation solar cells. Enormous research efforts have been invested to improve the efficiency of solar energy conversion which is determined by the light harvesting efficiency, electron injection efficiency and undesirable electron lifetime. A simple, cheap and trustable laser-induced photovoltage and photocurrent decay (LIPVCD) technique is adopted in this work in order to determine the electron lifetime (τ_e) and electron transport (τ_{tr}) in DSSCs. In LIPVCD technique, DSSC is illuminated by a small squared intensity-modulated laser beam. Time-based response of the DSSC is recorded using a transient digitized oscilloscope for further analysis. Frequency-based response was also investigated in this work. The frequency-dependent measurements turned out to be a powerful method to determine electron time constants in a fast, real-time fashion. Measurements were carried out using a standard dye-sensitized solar cell, and results were in excellent agreement with results obtained from traditional IMVS\IMPS measurements. Measurements were also performed for a variety of DSSCs, having various electrodes including TiO_2 nanoparticles, TiO_2 nanosheets with exposed {001} facets and ZnO vertically aligned nanowires. Results will also be presented and discussed in this work.

Keywords: DSSCs, electron lifetime, electron diffusion time

Nanoengineering: Fabrication, Properties, Optics, and Devices XII, edited by Eva M. Campo, Elizabeth A. Dobisz, Louay A. Eldada, Proc. of SPIE Vol. 9556, 955604 · © 2015 SPIE · CCC code: 0277-786X/15/$18 · doi: 10.1117/12.2185921

1. Introduction

Dye-sensitized solar cells (DSSCs) have been very promising as a new, low-cost alternative for solar energy harvesting devices [1]. The low-cost and solution-based fabrication of nanostructured electrodes of metal oxides (e.g. TiO_2, ZnO, SnO_2) is one of the main factors behind their success. The TiO_2 electrode, typically fabricated from 20-25 nm grains of TiO_2, using a simple solution-based and robust process acts as a high-surface-area scaffold where the light absorbing dye molecules are adsorbed. The TiO_2 electrode works after that as an efficient transport layer for electrons that are injected from the adsorbed dye molecules. Although it suffers from a large density of trapping defect states [2] that slows down the electron transport to the FTO anode, this slow-down in the transport process is balanced in time with the slow ionic motion of holes through the iodine electrolyte in the cell [3], and does not effectively deteriorate the solar cell dynamics. The only challenge caused by these traps is the high possibility that transported electrons can be lost via recombination with the surrounding electrolyte. In fact, electron recombination with electrolyte can be considered as the main recombination loss of collected electrons, defining therefore the electron lifetime in the TiO_2 layer [4]. Electron lifetime, τ_e, can be defined effectively by the time before the electron in the TiO_2 layer recombines with the electrolyte. The challenge, for an efficient solar cell device, is then to have the electron transport taking place in a time scale that is much shorter than its lifetime.

The morphology as well as material properties of the nanostructured metal oxide electrode play important roles in the determination of electron time constants. Columnar morphology (e.g. vertically aligned nanowires, nanotubes) of the electrode, for example, provides a direct path for electron transport, resulting in shorter diffusion to the FTO anode. The transport process is also determined by the material properties (dielectric constant, density of defects) of the electrode. Surface properties of the electrode are also important, as recombination of electrons with the electrolyte is mainly as surface process.

Many techniques have been developed for the measurements of both electron lifetime, and electron transport time in the TiO_2 layer in dye-sensitized solar cells. Optical based techniques have been used for this purpose, where a modulated light beam is used to develop a photovoltage, in open-circuit conditions, or a photocurrent, in short circuit conditions, and information about electron lifetime and electron transport time can be extracted, in frequency-domain or in time-domain, from the transfer function between the incident modulated light beam and the developed photovoltage and photocurrent.

Sinusoidal modulation of light has been used in photovoltage and photocurrent measurements, and these techniques are called intensity-modulated photovoltage spectroscopy IMVS and intensity modulated photocurrent spectroscopy IMPS, respectively [5-7]. In these techniques, a background DC light intensity is used to raise the quasi Fermi level of electrons in the TiO_2 layer to the specified level at which electron time constants are to be measured, and a small amplitude sinusoidal modulation is superimposed on the dc light background for the probing purpose. The amplitude of the ac modulation is set low enough that the quasi Fermi level does not effectively change during measurements. Electron time constants (lifetime and transport time) can then be calculated in the frequency domain from the frequency at which the phase lag between the response signal (photovoltage or photocurrent) and light modulation is maximum. At this characteristic frequency, the famous diffusion model predicts electron time constants from the simple formula [4]:

$$\tau = \frac{1}{2\,\pi\, f_{max}}$$

where f_{max} is the characteristic frequency. Electron lifetime is found from photovoltage measurements, while electron diffusion (or transport) time is found from photocurrent measurements.

On the other, square modulation of light intensity has been used but in time-domain measurements [8-9]. Here, a small amplitude ac light component superimposed a dc light background, and the photovoltage and photocurrent time decay transients are measured. Electron lifetime and diffusion time are found from exponential fitting of photovoltage and photocurrent decay transients respectively.

In this work, we adopt a simplified version of square modulation-based measurement system, where laser-induced photovoltage and photocurrent decay (LIPVCD) can be used to measure the electron lifetime and electron transport times, and where the modulation frequency can be freely swept in a real-time fashion. We show for the first time that a single illumination source can be used both for the dc light biasing and for the ac light modulation. The use of an external frequency function generator helped to have a fast real-time change of modulation frequency. Photovoltage and photocurrent transients have been recorded for different DSSC electrodes, namely: P25 TiO_2 nanoparticles, TiO_2 nanosheets with {001} exposed facets, and vertically aligned ZnO nanowires. We also investigated the frequency dependence of square modulation technique, and we show that frequency-based measurements can be perceptibly carried out using square modulation.

2. Experimental

2.1 Fabrication of DSSCs

DSSCs were prepared on SnO_2:F-coated glass substrates (12-13 Ω/square, 2.3 mm thickness). FTO glass plates were first cleaned in a detergent solution using an ultrasonic bath for 30 min and were then rinsed with deionized water and also with ethanol. Three kinds of working electrodes were fabricated under different conditions.

2.1.1 Fabrication of Metal Oxide Electrodes

P25 TiO_2 nanoparticles (SigmaAldrich) were used to make the first electrode. For the second electrode, TiO_2 nanosheets with exposed {001} facets were prepared according to a previously reported method [10]. Pastes of TiO_2 nanoparticles and TiO_2 nanosheets were fabricated after that. The method for paste preparation is reported elsewhere. The TiO_2 electrodes were then prepared by screen printing the fabricated pastes to make layers of ~ 12 μm thickness and area of 0.28 cm^2. The electrodes were sintered after that at 450 °C for 30 min. After cooling to 80 °C, the TiO_2 electrode was immersed into the N-719 dye solution (0.5 mM in ethanol) for 24 h.

The ZnO electrode was prepared by first dip-casting a solution of 0.01M of Zinc acetate dihydrate in ethanol. The dip-casting was performed 4 times on a well-defined 0.25 cm^2 area, and the dipped solution was allowed to dry between every two successive drops. The FTO substrate was then sintered at 350 ^oC for 30 minutes. After that, the dip-casting/sintering cycle was repeated again, allowing a better uniform coverage of the deposited seed layer. The prepared seed layer was immersed after that in the growth solution (25 mM Zinc Nitrate and Hexamine in DI-water) and put in the oven at 90^oC for 2 hours. This resulted in a layer of vertically aligned ZnO nanowires of ~ 30 nm diameter and ~ 500-600 nm length. After cooling to room temperature, the ZnO nanowire electrode was washed with DI-water, and sintered on the hotplate at 400 ^oC. After that, it was immersed into the N-719 dye solution (0.5 mM in ethanol) and was held at room temperature for 1 h, followed by washing with water and ethanol.

2.1.2 Preparation of Counter Electrodes, DSSCs Fabrication and Efficiency Characterization

For the counter electrodes, the FTO plates were coated with a drop of 10 mM H_2PtCl_6 solution and were then heated at 400 °C for 30 min. Dye-coated TiO_2 and ZnO nanowire layers, and Pt counter electrodes were assembled into sandwich-type cells. An electrolyte solution (Dysole HPLSE) was injected between the counter electrodes. Photovoltaic I-V measurements on the fabricated DSSCs were performed under an AM 1.5 solar simulator.

2.2 Laser-induced Photovoltage and Photocurrent Decay (LIPVCD) Setup

Electron lifetime and electron transport time were measured by laser induced photovoltage and photocurrent decay technique (LIPVCD). A high-power semiconductor diode laser (532 nm, 40 mW) was used as the light source in these studies. The diode laser was controlled using MELLES GRIOT 06 DLD 105 diode laser controller, and it was externally modulated using a square frequency generator. The small square wave-modulated laser beam was always incident on the working electrode side of the solar cell. The photovoltage and photocurrent response of the solar cell was traced using a digital oscilloscope.

The solar cell connection setup for the photocurrent decay is shown in Fig.1. The cell terminals are connected to an external load (50Ω resistance) and the terminals of the resistance is connected directly to the digital oscilloscope. The laser modulation frequency is set to an enough value so that the photocurrent decays and rises between two steady-states [5]. The modulation amplitude was kept always less than 10% in order to ensure linear response dynamics from the solar cell. From the ensuing decay, the transport time is extracted. When the DSSC is illuminated with a small square-wave modulation superimposed on a steady-state illumination, the photocurrent decays from a high steady state value, I_h, to a lower steady state value, I_ℓ, provided that the modulation period is long enough compared to the time constant of the decay. The experimental setup of the photovoltage decay measurement was the same as in photocurrent decay arrangement but the cell terminals are connected directly to the oscilloscope without the external load resistance.

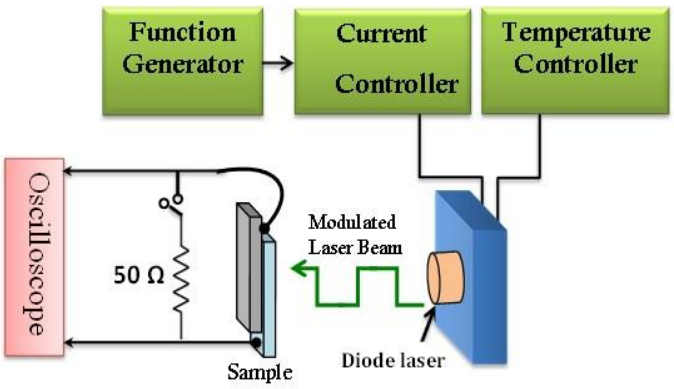

Figure 1: Schematic of setup used for LIPVCD measurements

3. Results and discussion

3.1 Comparison between TiO_2 nanoparticles and TiO_2 nanosheets with exposed {001} facets

Figure 2 and Table 1 show the I-V characteristics of the solar cell devices fabricated using the P25 nanoparticles and TiO_2 nanosheets. The P25 cell showed a higher Isc and Voc of 13.9 mA/cm^2 and 0.73 V respectively. The nanosheet sample showed a higher fill factor of 0.55, compared to 0.45 of nanoparticle cell, but Isc and Voc were reduced (11.8 mA/cm^2 and ~0.7 V respectively). The interesting point is that although TiO_2 nanosheets are reported to show better dye loading [11], we find here that both generated photocurrent and photovoltage are reduced. We attribute this reduced performance in TiO_2 nanosheet sample to either reflection losses resulting from the planar morphology of TiO_2 nanosheets, the reduced transport in nanosheets resulting also from their morphology, and to probably lower dye loading resulting from different ambient and preparation conditions of TiO_2 electrodes reported in the literature.

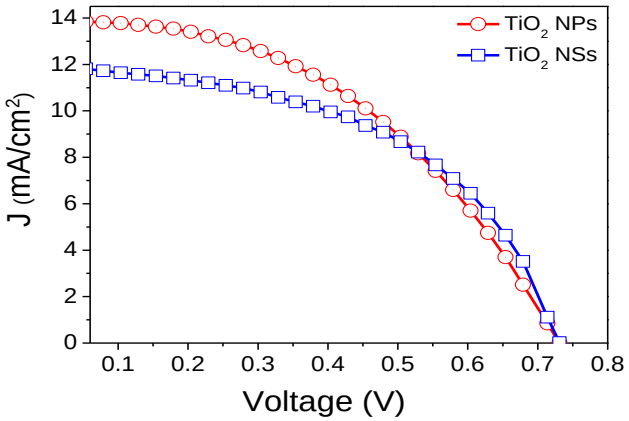

Figure 2: Current density–Voltage curves of DSSCs based on TiO_2 nanoparticles (red circles) and TiO_2 nanosheets (blue squares) under standard AM 1.5G illumination.

Table 1: Detailed photovoltaic parameters of DSSCs based on different TiO_2 photoanodes measured under one sun illumination (AM 1.5G, 100 mW cm^{-2}). J_{SC}: short-circuit photocurrent density; V_{OC}: open-circuit photovoltage; FF: fill factor; η: photovoltaic conversion efficiency.

Cell	J_{SC} (mA/cm^2)	V_{OC} (V)	FF	η (%)
TiO_2 NP	13.9	0.731	0.451	4.7
TiO_2 NS	11.83	0.696	0.55	4.53

Laser induced photovoltage and photocurrent decay (LIPVCD) technique was employed to further investigate the charge dynamics in the fabricated cells, and results are shown in figure 3. Figure 3a shows typical photocurrent and photovoltage decays for a working device, where the longer photovoltage decay resembles a recombination time that is longer enough than the transport time presented by the photocurrent decay in the same graph. The electron lifetime was plotted for both samples in figure 3b at different light intensities. As can be seen in the figure, both samples have very long lifetimes at low intensities, but at higher intensities, nanosheets show better performance with a longer lifetime. This will of course result in better charge collection efficiency in the device. The transport time was measured, from photocurrent measurements, and is shown in figure 3c. Clearly, nanosheets have longer transport time, while NPs

showed a shorter transport time. We attribute this reduced electron dynamics of nanosheets to their planar morphology that will result in wider grain boundaries between adjacent nanosheets, unlike nanoparticles that have less contact area between the nanoparticles. This can also be the reason behind the reduced Voc in the nanosheet sample.

The diffusion length was calculated form the measured electron lifetime and electron transport time taking into consideration the measured electrode thicknesses of prepared samples, and interestingly it gave similar diffusion lengths of 16 µm for NPs and 13 µm for nanosheets at a light intensity of ~ 25 mW/cm^2, as can be seen in Table 2. Therefore, while electron transport was better for NPs, this was compensated by longer electron lifetime resulting in comparable diffusion lengths between the two samples. For ZnO nanowires, we had a poor electron transport time of ~ 0.5 ms for a nanowire of 1 µm long, although the lifetime was as long as 53 ms, resulting in diffusion length of ~ 26 µm, which makes ZnO nanowires promising for further studies. We attribute the poor transport to the quality of the solution-processed seed layer.

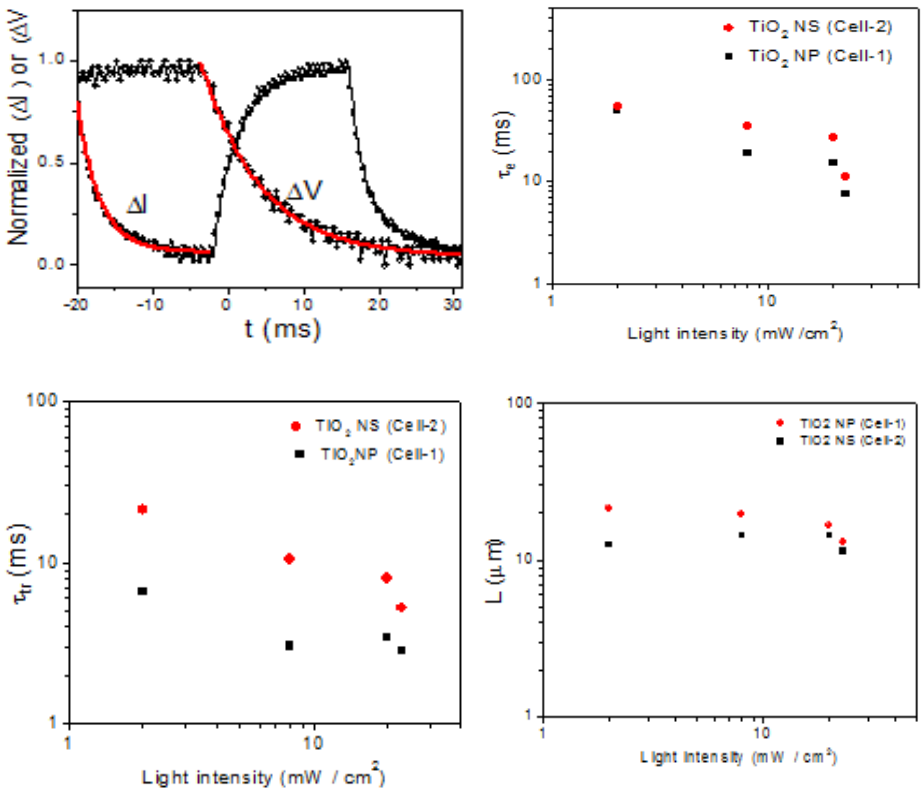

Figure 3 (a) An example of photovoltage decay (ΔV) and photocurrent decay (ΔI) for the TiO_2 NP DSSC under square modulated beam 23 mW/cm^2. The red curves represent the exponential decay fitting of the data; (b) Electron lifetime (τ_e) as a function of the light intensity; (c) Electron transport lifetime (τ_{tr}) as a function of light intensity. The data were extracted from the exponential fitting of the transient photovoltage and photocurrent decays for the two cells; (d) the values of diffusion length (L), calculated from (τ_{tr}), (τ_e), and the film thickness, as a function of the light intensity.

Table 2: Characteristics of electron transport times, lifetimes, diffusion coefficient and electron diffusion length with the three samples.

DSSCs	Thickness (μm)	τ_e(ms)	τ_{tr}(ms)	D_n (cm^2s^{-1})*10^{-4}	L_n (m)*10^{-6}
NPs	12	5.2	1.26	4.86	16
NSs	10	7.86	2	2.13	13

3.2 Frequency-based Measurements using square-modulated light intensity

Traditionally, small amplitude *square* light modulation (with the presence of a dc background light intensity) provides a direct means to measure electron lifetime and diffusion time through the photovoltage and photocurrent transients following light modulation.

On a principally another hand, small amplitude *sinusoidal* modulation has been also used for such measurements, but in a totally different method. In the sinusoidal modulation-based IMVS and IMPS techniques, electron time constants are expected from the trapping/detrapping diffusion model to correspond to the frequencies at which the photovoltage and photocurrent signal lags maximum behind light modulation.

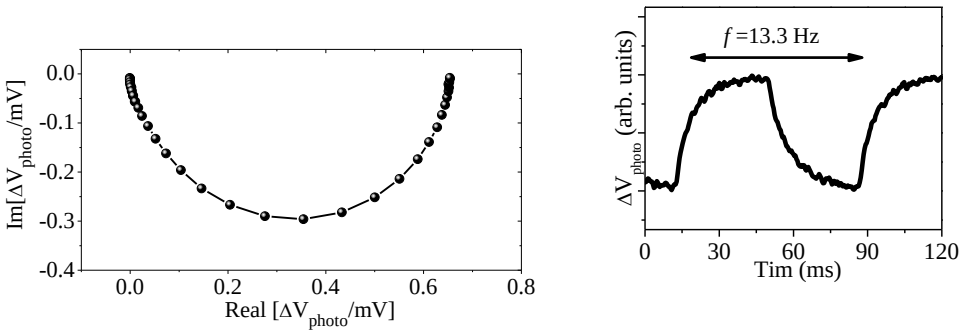

Figure 4: (a) IMVS response of the DSSC at different light intensities (b) DSSC photovoltage response under square modulation with dc light intensity of 20 mW/cm^2.

In our work, we also show for the first time that frequency dependence in square modulation techniques can also be invoked in the same way, and that electron time constants can similarly be expected from the diffusion model. The beauty of our technique is that, compared to other techniques, it provides a very rapid and real-time method to determine electron time constants. Our results for photovoltage measurements are shown in figure 4. Figure 4a shows the IMVS response at light intensity of 20 mW/cm^2, and figure 4b shows the generated photovoltage decay at the same light

intensity. The photovoltage decay reaches saturation level exactly at the same frequency that has the maximum phase lag in IMVS response. Investigations of saturation level achievement criteria and error limits for this new technique are under progress by our group.

4. Conclusion

We presented a laser-induced photovoltage and photocurrent decay (LIPVCD) technique that uses a single illumination source, and an easily tunable light modulation by the external modulation of laser diode controller using a simple frequency generator. We test DSSC cells with different TiO_2 electrodes using this setup, and we showed a detailed comparison between P25 TiO_2 nanoparticles and TiO_2 nanosheets with exposed {001} facets. The NP cell showed a shorter electron lifetime but a faster electron transport time resulting in similar diffusion lengths between the two cells. We also showed for the first time that our setup allows frequency-domain measurements, along with time domain ones, in a fast real-time fashion, thanks to the external frequency function generator used in the setup. Further investigations are also currently under progress.

References

[1] O'Regan B. and Grätzel, M., "A low-cost, high-efficiency solar cell based on dye-sensitized colloidal TiO_2 films," Nature, 353, 737-740 (1991)

[2] Bisquert, J., "Chemical capacitance of nanostructured semiconductors: its origin and significance for nanocomposite solar cells," Phys. Chem. Chem. Phys., 5, 5360-5364 (2003)

[3] Kopidakis, N., Benkstein , K.D., van de Lagemaat, J., Frank, A.J., "Transport-Limited Recombination of Photocarriers in Dye-Sensitized Nanocrystalline TiO_2 Solar Cells," *J. Phys. Chem. B*, 107 (41), 11307–11315 (2003)

[4] Kalyanasundaram, K., [Dye-Sensitized Solar Cells], EPFL Press, Lausanne, Chapter 10 (2010)

[5] Cao, F., Oskam, G., Meyer, G. J., Searson, P. C., "Electron Transport in Porous Nanocrystalline TiO_2 Photoelectrochemical Cells," *J. Phys. Chem.*, 100, 17021–17027 (1996)

[6] Schlichthörl, G., Huang, S. Y., Sprague, J., Frank, A. J., "Band Edge Movement and Recombination Kinetics in Dye-Sensitized Nanocrystalline TiO_2 Solar Cells: A Study by Intensity Modulated Photovoltage Spectroscopy," *J. Phys. Chem. B*, 101, 8141–8155 (1997)

[7] Dloczik, L., Ileperuma, O., Lauermann, I., Peter, L. M., Ponomarev, E. A., Redmond, G.,Shaw, N. J., Uhlendorf, I., "Dynamic Response of Dye-Sensitized Nanocrystalline Solar Cells: Characterization by Intensity-Modulated Photocurrent Spectroscopy," *J. Phys. Chem. B*, 101, 10281–10289 (1997)

[8] Nakade, S., Kanzaki, T., Wada, Y., Yanagida, S., "Stepped Light-Induced Transient Measurements of Photocurrent and Voltage in Dye-Sensitized Solar Cells: Application for Highly Viscous Electrolyte Systems," *Langmuir*, 21, 10803–10807 (2005)

[9] van de Lagemaat, J., Frank, A. J., "Nonthermalized Electron Transport in Dye-Sensitized Nanocrystalline TiO_2 Films: Transient Photocurrent and Random-Walk Modeling Studies," *J. Phys. Chem. B*, 105, 11194–11205 (2001)

[10] Han, X., Kuang, Q., Jin, M., Xie, Z., Zheng, L., "Synthesis of Titania Nanosheets with a High Percentage of Exposed (001) Facets and Related Photocatalytic Properties," *J. Am. Chem. Soc.*, 131 (9), 3152–3153 (2009)

[11] Fan, J., Cai, W., Yu, J., "Adsorption of N719 dye on anatase TiO_2 nanoparticles and nanosheets with exposed (001) facets: equilibrium, kinetic, and thermodynamic studies," *Chem. Asian J.*, 6 (9), 2481–2490 (2011)